Analyst

PAPER

View Article Online
View Journal | View Issue

Cite this: *Analyst*, 2024, **149**, 5684

Capillary-flow driven microfluidic sensor based on tyrosinase for fast user-friendly assessment of pesticide exposures†

Claire E. Hefner, [a] Prakash Aryal, [a] Eric Brack,[b] Todd Alexander[b] and Charles S. Henry *[a,c,d]

Pesticides are primarily used in agriculture to protect crops and extend their longevity. However, pesticide exposure has been linked to various acute and chronic health effects, raising significant environmental concerns. Current detection methods are often expensive and time-consuming, relying on complex instruments. Although enzyme-inhibition-based microfluidic paper-based analytical device (mPAD) platforms offer an easier alternative, they suffer from slow analyte transport and analyte adsorption issues in microchannels. Consequently, there is a need for a fast, simple, and cost-effective point-of-need platform for pesticide sensing. In this study, we present a rapid microfluidic platform for on-site pesticide residue detection. Unlike traditional mPAD platforms, our system transports pesticide samples through hollow capillary channels within seconds without adsorption of pesticides in the microchannels. While much research has focused on acetylcholinesterase inhibition on paper, this study is the first to introduce a tyrosinase inhibition-based assay on a paper platform for pesticide detection. Ziram, a representative dithiocarbamate pesticide, was detected using a colorimetric enzymatic inhibition assay. A limit of detection (LoD) of 1.5 ppm was obtained. In this study, we optimized the fast-flow device, assessed its stability and susceptibility to various interferences, and conducted real-sample tests using glove extraction to evaluate its capability in real-world settings. Spike recovery analysis revealed an extraction efficiency of 82.5% to 87.5% for leather gloves and 68.9% to 71.9% for nitrile gloves. This platform demonstrates strong selectivity against interferences, with the enzyme retaining 90% activity even after a week under the established storage protocols with room for further investigation. While primarily a proof of concept, this device shows promise as an additional tool for pesticide detection, with potential future integration into multiplexed devices.

Received 10th September 2024,
Accepted 28th October 2024

DOI: 10.1039/d4an01203h

rsc.li/analyst

Introduction

The use of pesticides in agriculture has grown significantly in recent decades, with over 2.7 million tons used worldwide in 2020 alone.[1] This number has nearly doubled over the last 30 years.[1] Pesticides are extensively employed in agricultural practices, effectively controlling pests and significantly boosting crop yields. However, their widespread application raises significant environmental and health concerns.[2,3] Non-target exposure to pesticides has been linked to a host of health issues, including cancer, asthma, neurological diseases, and hormone disruption.[4]

Pesticide handlers face some of the highest risks, frequently encountering pesticides through spraying, mixing, and handling treated crops.[4,5] Studies indicate an estimated 385 million cases of unintentional pesticide poisoning (UAPP) globally every year.[6] Moreover, it has been reported that over 200 000 people die each year from pesticide poisoning, with a significant portion of these cases involving active pesticide handlers. To minimize the effects of pesticide exposure, understanding where and when exposure is occurring is important. To do this, we must employ precise methods to measure pesticides on-site at the place of application.[7]

Dithiocarbamate (DTC) pesticides, primarily used as fungicides to control fungal diseases in various crops, are a class of pesticides consumed globally in large quantities, ranging

[a]*Department of Chemistry, Colorado State University, Fort Collins, Colorado 80523, USA. E-mail: chuck.henry@colostate.edu*
[b]*U.S. Army Combat Capabilities Development Command (DEVCOM)-Soldier Center, 10 General Greene Avenue, Natick, Massachusetts 01760, USA*
[c]*Department of Chemical and Biological Engineering, Colorado State University, Fort Collins, Colorado 80523, USA*
[d]*School of Biomedical Engineering, Colorado State University, Fort Collins, Colorado 80523, USA*

† Electronic supplementary information (ESI) available. See DOI: https://doi.org/10.1039/d4an01203h

between 25 000 and 35 000 metric tons annually.[8] Common DTC pesticides include Ziram, Thiram, and Mwhancozeb.[9] Exposure to DTC residues has been associated with neurological disorders such as Parkinson's disease and abnormal thyroid function.[8] Moreover, DTCs can degrade into ethylene thiourea, a known carcinogen.[8] Therefore, targeting DTCs for detection is crucial due to their potential threat to human health, especially for those who handle pesticides directly.

Despite the clear need for rapid monitoring, current pesticide detection methods, such as gas chromatography-mass spectrometry (GC-MS) and liquid chromatography-mass spectrometry (LC-MS), are sensitive and selective but not suitable for on-site testing. These conventional techniques are costly, time-consuming, require trained personnel, and need centralized laboratories, limiting their accessibility for rapid and efficient monitoring. Therefore, there is a need for a portable, rapid, user-friendly device for screening large amounts of samples, which can be followed by traditional chromatographic methods.

Paper-based microfluidic devices offer a promising solution, providing a cost-effective and accessible platform for onsite pesticide detection.[10–12] These devices rely on capillary action for passive fluid flow and can handle microliter volumes of fluid, making them ideal for resource-limited settings. Various devices for pesticide detection have been developed, primarily using enzyme-based inhibition as the operational mechanism.[13,14] Other explored probes include optical and electrical sensors based on nanomaterials,[15,16] antibodies,[17] aptamers,[18] and molecularly imprinted polymers (MIPs).[19] Optical sensing is ideal for field-based applications, requiring minimal external instrumentation, with color changes visible to the naked eye or a smartphone.[20] However, there is currently limited work on fast-flow microfluidic devices for this application space.

While acetylcholinesterase (AChE) is the most commonly used enzyme in these assays, other enzymes, such as butyrylcholinesterase, alkaline phosphatase, organophosphorus hydrolase, and aldehyde dehydrogenase, are also inhibited by certain pesticides.[13] Besides the aspect of limited specificity, Ziram inhibits AChE through a non-specific inhibition mechanism, including reversible inhibition.[21] Therefore, a model based on AChE activity determination becomes limited. Building on our previous work, where we developed protocols for AChE inhibition on paper substrates using fast-flow microfluidics,[22] this study explores the use of tyrosinase as an alternative enzyme for detecting DTC. Tyrosinase is a type-3 copper protein; its active site contains two copper atoms, with each atom coordinated to three histidine residues.[23] Tyrosinase catalyzes phenols to *ortho*-quinones *via* monooxygenation, and catechols to *ortho*-quinones *via* oxidation.[23] Its primary function is catalyzing the first step of melanin biosynthesis, a pigment in the body, and is the cause of the browning of fruits/vegetables. Previous work has documented the use of tyrosinase for pesticide detection, and records show tyrosinase is inhibited by carbamates and dithiocarbamate pesticides, atrazine, chlorophenols, and thioureas.[13] Additionally, when compared to AChE, tyrosinase tends to demonstrate higher stability due to its copper complexation and disulfide bonds.[24] Wang *et al.* developed an assay for DTC pesticide detection using enzymatic inhibition, with tyrosinase as an enzyme probe.[25] This assay uses catechol as the substrate and 4-amino-antipyrine (4AAP) as a secondary reagent in solution. Guo *et al.* further enhanced this method with a solvent-based tape extraction for detecting DTCs in food samples.[26] Although both studies demonstrated strong analytical performance, they relied on UV-Vis spectroscopy for detection, which is impractical for point-of-need testing due to its complexity, cost, and operational requirements. To date, there have been no reports using tyrosinase-based pesticide assays in low-cost capillary flow microfluidic devices.

To address these challenges, we developed a fast-flow microfluidic sensor that combines the tyrosinase assay with microfluidics for colorimetric detection of DTC pesticides. This device offers increased portability, faster analysis times, reduced sample volume requirements, and potential automation of the detection process. Our device, in contrast to conventional paper-based platforms, moves pesticide samples *via* hollow capillary channels in a matter of seconds without the pesticides adhering to the microchannels. This study is the first to present a tyrosinase inhibition-based test for pesticide detection on a paper platform, although acetylcholinesterase inhibition has been the subject of extensive research. Additionally, we demonstrate the device's potential for understanding pesticide handlers' exposure by testing Ziram extraction on various gloves, which handlers commonly use. By leveraging microfluidic technology, this approach broadens detection capabilities and paves the way for potential multiplexed pesticide detection on fast-flow microfluidic systems.

Experimental

Chemicals and materials

Ultrapure water from a Milli-Q system (Merck Millipore Darmstadt, Germany, R 18.2 MΩ cm) or ethanol were used to prepare all solutions unless otherwise noted. Tyrosinase (400 U mL^{-1}), catechol (1 g L^{-1}), and 4AAP (3 g L^{-1}) were used for assay experiments. Tyrosinase from mushrooms was used as an enzyme. The tyrosinase solution, catechol, and 4AAP solutions were all prepared in phosphate-buffered saline (PBS) (50 mM, pH 6.5) from PBS tablets (NaCl, KCl, Na_2HPO_4, KH_2PO_4). The Ziram pesticide solution was prepared in an aqueous ethanol solution (30% v/v EtOH/H_2O) with concentrations of Ziram ranging from 0.1 to 100 ppm. All chemicals were purchased from Sigma-Aldrich (St. Louis, MO, USA) except as noted above. All chemicals were used without further purification. Catechol and 4AAP solution were made fresh every day at room temperature. Double-sided adhesive (468MP), glass fibers, and PET transparency film (9984) were obtained from 3M, St. Paul, MN, USA. Whatman grade 1 filter paper was purchased from Fisher Scientific, Hampton, NH. The premium cowhide leather palm gloves were purchased

from G&F Products, Inc. (Philadelphia, PA). Materials for the device were cut with a CO_2 laser (Epilog Zing, Golden, CO, USA).

Device fabrication

The capillary-driven microfluidic device consists of three inlets, three microfluidic channels, and three outlets (Fig. 1). The device is composed of three layers and was fabricated by laminating alternating sheets of 9984 transparency film and double-sided adhesive.[27–30] A CO_2 laser was used to cut patterns in each layer of the device to form the hollow microchannels, inlet, and outlets. The bottom of the device contains the detection zone, which is folded over onto the outlets during operation. During assembly, glass fiber (6 mm diameter) and Whatman 1 (8 mm diameter) paper circles are cut and added into their designated areas on the device for the pretreatment of reagents. Tyrosinase (12.5 μL) was dried on each glass fiber circle, and catechol and 4AAP (2 : 1, 7.5 μL) were dried on each paper circle. PVC was added to the bottom detection zone area of the device to help with imaging, as it provides a uniform and non-reflective surface for capturing images. The full device measures 5 cm × 3.3 cm and is 3.4 × 3.3 cm after folding at the dotted line. Each flow channel measures 17 mm × 2.5 mm.

Assay operation

The enzyme and substrates were dried onto each glass fiber and Whatman 1 circles respectively and left to dry at room temperature. After complete drying (approximately 30 minutes), 20 μL of Ziram solution was pipetted into each microfluidic channel inlet. The Ziram solution flowed through the channels and completely saturated the glass fiber pads. The Ziram solution was then incubated with the tyrosinase in the glass fiber pads for 3 min. Following the incubation step, the top part of the device was folded down on top of the glass fiber circles to ensure complete contact with catechol/4AAP pretreated circles, which initiates the enzymatic reaction. After 10 min, an image of the device was captured using a smartphone inside of a lightbox. Color formation begins seconds after folding (see ESI video†), however capturing an image 10 min after folding ensures the most color development and a maximum signal (as shown in Fig. 3B).

Image analysis

The images of the paper circles on the device were taken using a smartphone camera under controlled light conditions. Images were analyzed in ImageJ (NIH). First, the image was split into its color channels (Red, Green, Blue). The green channel was then selected for analysis as it had the highest intensity (see ESI, Fig. S1†). The green channel image was then inverted to decrease the background noise. A circular region of interest (ROI) was selected on the paper pads, and the mean grayscale was averaged between the three ROIs. The mean grayscale value was used to quantify the color intensity of each circle and directly relates to the Ziram concentration present in the sample solution. Details for the ImageJ analysis are found in the ESI (see ESI, Fig. S2†).

Results and discussion

Assay principle

The proposed chromogenic reaction mechanism carried out inside the device is shown in Fig. 2. It has been adapted from a previous study.[25] Tyrosinase has four oxidation states: met-, oxy-, deoxy-, and deact-tyrosinase.[23] Oxidation of catechol to *ortho*-quinone occurs *via* oxy-tyrosinase to met-tyrosinase, where catechol initially binds to the active site through the CuB atom.[23] The binding takes place by the deprotonation of the hydroxyl groups on catechol; the oxygens are then co-ordinated with the two active site copper atoms.[23] The complex then dissociates with the release of the oxygen atoms from the peroxy-conformation, forming the *ortho*-quinone.[23] The active site copper ions are Cu(II). After the tyrosinase enzyme oxidizes the catechol substrate, the *ortho*-quinone

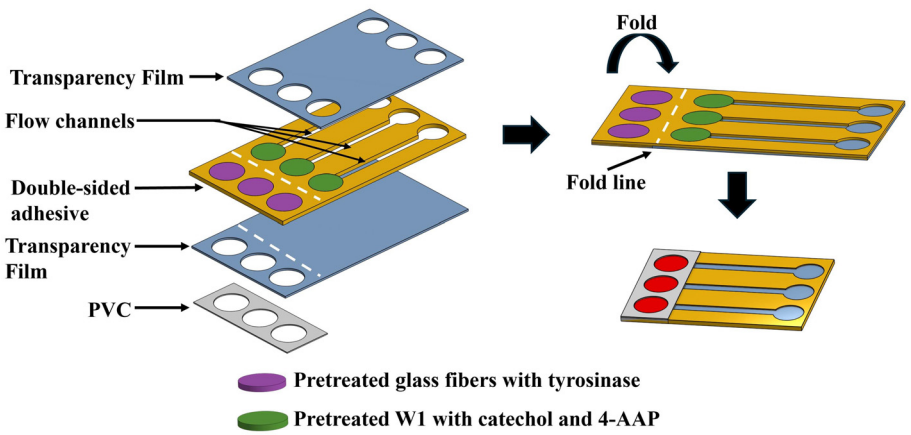

Fig. 1 Device assembly schematic and running procedure. After adding the sample, it incubates with the enzyme for three minutes. The top of the device is then folded down, initiating the reaction between the enzyme and substrate, which results in color formation.

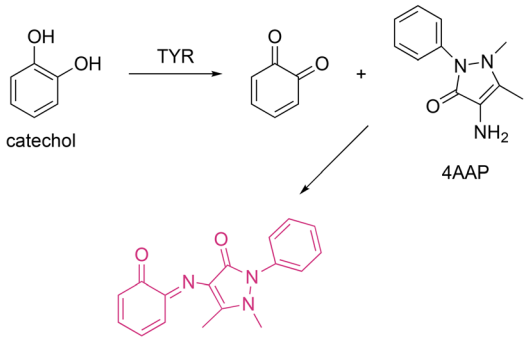

Fig. 2 Proposed chromogenic reaction mechanism with tyrosinase (TYR), catechol, and 4AAP reagents.[25] Reprinted (adapted) with permission from ref. 25 Copyright {2020} ACS.

reacts with 4-aminoantipyrine (4AAP) to form a colored product (Fig. 2). In the presence of Ziram, a representative dithiocarbamate (DTC) pesticide, tyrosinase catalytic activity is inhibited, decreasing the amount of colored product formed. The color change is inversely proportional to the amount of Ziram present in the sample. Therefore, Ziram concentration can be quantitatively determined through image capture analysis.

Sensor performance

The device performance was optimized through various parameters, including tyrosinase concentration, catechol concentration, 4AAP concentration, and reaction time (Fig. 3A). In the working assay, the color reduction results from inhibited tyrosinase enzyme activity due to the presence of pesticides. Therefore, optimizing the initial tyrosinase concentration on the device is crucial. Tyrosinase concentrations ranging from 250 to 500 U mL^{-1} (250, 300, 350, 400, 450, and 500 U mL^{-1}) were tested, and mean grayscale intensity was examined for each concentration. This broad range was selected because each concentration produced distinct variations in signal, whereas narrower ranges failed to show significant differences in response. The blank and tests were compared for each tyrosinase concentration. Generally, the signal intensity increased with higher tyrosinase concentrations.

Interestingly, 500 U mL^{-1} tyrosinase did not follow the trend where higher enzyme concentration corresponds to a higher signal (Fig. 3A). This result could be due to tyrosinase

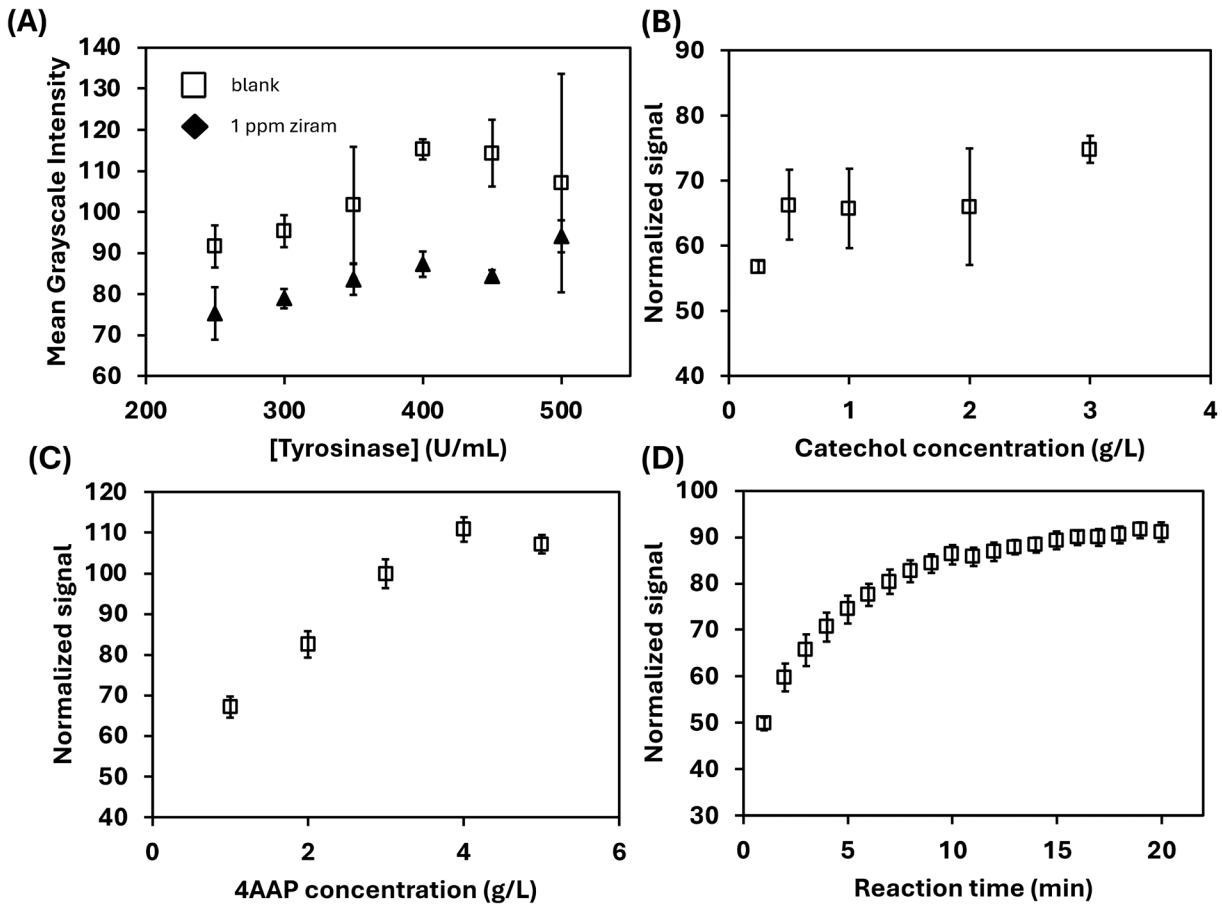

Fig. 3 Assay optimization for pesticide analysis (n = 3). (A) Tyrosinase concentration plotted against mean grayscale intensity. (B) Catechol concentration plotted against the normalized signal. (C) 4AAP concentration plotted against the normalized signal. (D) Reaction time plotted against the normalized signal. The optimized conditions were determined to be 400 U mL^{-1} tyrosinase, 10-minute reaction time, 1 g L^{-1} catechol, and 3 g L^{-1} 4AAP.

becoming its own inhibitor at high concentrations.[31] Additionally, at 500 U mL^{-1} enzyme concentration, there may be no additional catechol in the solution to bind, however, this is unlikely as the substrate concentration is extremely high compared to tyrosinase. Another possibility is that tyrosinase can occasionally process catecholic substrates as phenols, oxidizing them by the monooxygenase pathway.[23] This can lead to the reductive elimination of one of the active-site copper ions in the tyrosinase active site and the conversion of oxy-tyrosinase to inactive deact-tyrosinase [Cu(II)Cu(0)].[23] This process is independent of the product concentration and a function of the amount of tyrosinase initially present.[23] Therefore, 400 U mL^{-1} tyrosinase was selected as the optimal concentration as although 450 U mL^{-1} also showed a high signal, having a higher enzyme concentration might increase the chances of tyrosinase inactivation by incorrect catechol processing, decreasing the efficiency of the assay. Additionally, 400 U mL^{-1} provided the highest signal in the blank and the lowest standard deviation. Finally, this concentration offered the most sensitive response between the blank and the test sample.

Next, catechol and 4AAP concentrations were optimized, as these compounds are the substrate and secondary reactant, respectively, contributing to the speed and sensitivity of the assay (Fig. 3B and C). Varying catechol concentrations from 0.25 g L^{-1} to 3 g L^{-1} (0.25, 0.5, 1, 2, and 3 g L^{-1}) showed little to no difference in signal intensity besides a noticeable decrease in intensity for 0.25 g L^{-1}; therefore, 1 g L^{-1} catechol was selected as the optimal concentration. This suggests that catechol concentrations above 1 g L^{-1} do not significantly enhance the assay's performance, indicating a saturation point where additional substrate does not contribute to increased signal. For 4AAP concentrations of 1 g L^{-1} to 5 g L^{-1} (1, 2, 3, 4, and 5 g L^{-1}), the normalized signal appeared to increase with higher concentrations of 4AAP. However, upon visual examination of the devices, there was hardly any noticeable difference in color intensity between 3 and 4 g L^{-1} 4AAP. This discrepancy between the quantitative signal and visual observation suggests that while the assay's sensitivity may improve slightly with higher 4AAP concentrations, the practical difference is minimal. Thus, 3 g L^{-1} was selected as the optimal 4AAP concentration, balancing the need for a measurable signal with the practicality of visual detection.

Finally, the assay reaction time, which is the duration the assay was allowed to produce color, was optimized (Fig. 3D). Immediately upon folding the device, images were captured every minute to monitor the normalized signal over time. 10 minutes was selected as the optimal image capture time, as by this point, the signal intensity started to level off. Overall, the optimal conditions for the pesticide analysis assay were 400 U mL^{-1} tyrosinase, 1 g L^{-1} catechol, 3 g L^{-1} 4AAP, and 10 min reaction time.

Effect of solvent. The effect of solvent on the assay was also investigated (ESI, Fig. S3–S5†), as solvents are known to affect enzyme activity. Solvent type is also crucial for extraction efficiencies in field applications. Four solvents—methanol, ethanol, isopropanol, and DMSO—were tested in the assay at varying ratios with PBS (100%, 70/30, 50/50, 30/70) (Fig. S3†). A 30/70 (ethanol/water) mixture was selected as it showed the highest difference between the test and blank samples, with the least impact on enzyme activity (Fig. S5†). Ethanol is the least toxic and harmful solvent among those tested, making it a safer choice for field use and handler application. Moreover, the concentration of tyrosinase used is relatively high, which helps prevent significant denaturing of the enzyme. Further information on this study as well as the optimal paper type is included in the ESI (Fig. S3–S5 and Table S1† respectively).

Calibration

Calibration curves were plotted for the change in intensity ($I_{blank} - I_{test}$) *vs.* Ziram concentration (Fig. 4A) and percent inhibition *vs.* Ziram concentration (Fig. 4B) for the range of 0 ppm to 50 ppm Ziram (0, 0.1, 0.5, 1, 5, 10, 20, and 50 ppm) respectively. Both plots explore the relationship between Ziram concentration inhibition levels, showing an increase in inhibition with an increase in pesticide concentration. Additionally, both curves depict nonlinear behavior. The limit of detection (LoD) and limit of quantification (LoQ) were calculated to be 1.5 ppm and 5.0 ppm respectively. LoD was calculated using the three times standard deviation (SD) of the blank divided by the slope of the calibration curve.[32] LoQ was calculated by 10 times the SD of the blank divided by the slope.[32] A clear visual difference can be seen at 0.5 ppm for Ziram. In the USA, the maximum residue limit for Ziram is 7 ppm defined by International Agency for Research on Cancer (IARC), making our LoD within the relevant range.[33]

Interference study

To study the effect of interference of non-target compounds on the assay, standards of atrazine, paraoxon, Mn^{2+}, Fe^{3+}, Co^{2+}, Ni^{2+}, Zn^{2+}, Pb^{2+}, S^{2-}, Mg^{2+}, Na^{+}, Cu^{2+}, Cl^{-}, PO_4^{3-}, K^{+}, NO_3^{-}, glucose, and glutamic acid were prepared. The potential interferences were studied at a 1 : 1 ratio with 10 ppm Ziram (Fig. 5). As previously reported, other pesticides can have an inhibitory effect on the same type of enzymes.[34] Additionally, heavy metals are known to inhibit enzyme catalysis capabilities, therefore they were also examined.[35] Nutrients are commonly found and used in agriculture settings, so they were tested to see if they had any effects. Finally, glucose and glutamine acid were examined. Glucose was examined as it has been reported to indirectly inhibit tyrosinase activity by conversion into lactic acid.[36] Meanwhile, glutamine acid has also been reported to inhibit tyrosinase as a mixed-type inhibitor.[37] A wide range of potential interferents was tested to cover most possible environments in which the device might be used in the future, including agricultural settings, homes, food samples, and more. Overall, none of the non-target compounds exhibited a significant interference, as the inhibition from these non-targeted analytes was within ±10%.

Device stability

Devices were fabricated as described above. Devices were tested under two storage conditions, 5 °C and −20 °C. For

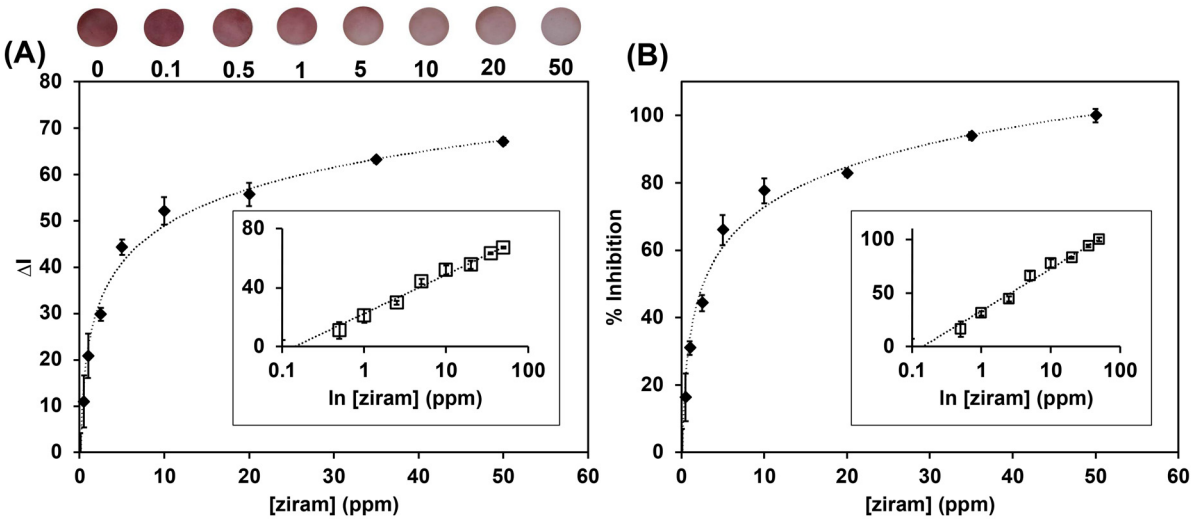

Fig. 4 Calibration curves for the assay on the device. Both qualitative (top) and quantitative (bottom) color analysis were observed. (A) Ziram concentrations from 0 to 50 ppm were tested and plotted against the change in intensity (blank − sample). The error bars indicate the standard deviation between three replicates. The exponential fit was calculated to be $y = (11.5 \pm 0.5)\ln x + (22.4 \pm 1.2)$ with an R^2 value of 0.99. (B) Ziram concentration *vs.* percent inhibition was also plotted and fit to the equation $y = (17.1 \pm 0.7)\ln x + (33.4 \pm 1.7)$ with an R^2 value of 0.99.

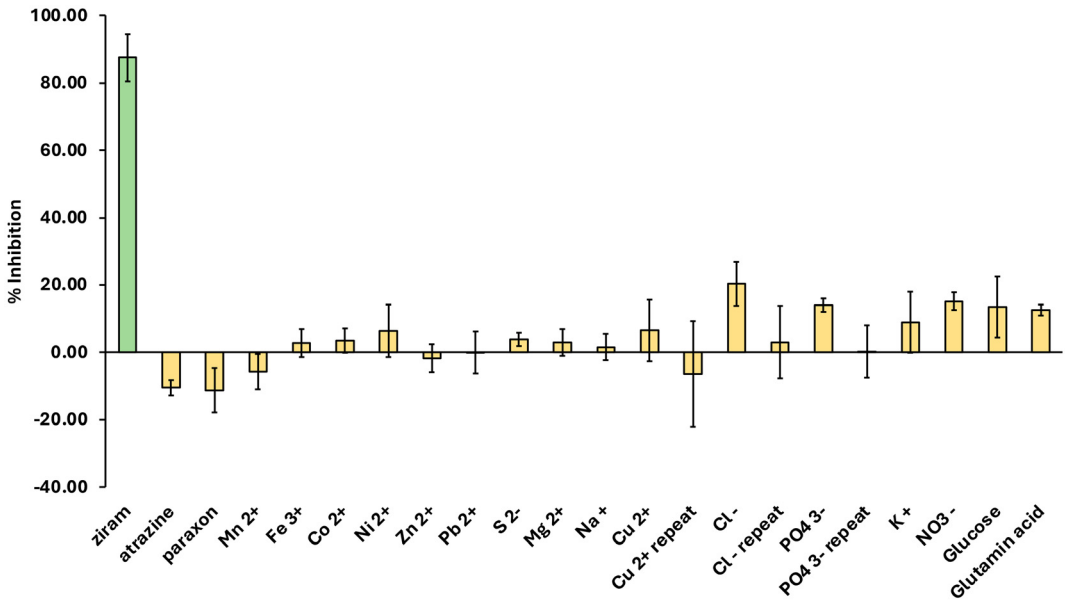

Fig. 5 Interference testing for the tyrosinase-Ziram assay for the developed sensor. The green bar indicates the control group (only Ziram) and the yellow bars indicate the other non-targeted analytes. Only Ziram showed a significant level of inhibition. The error bars indicate the standard deviation between three replicates.

each condition, some devices were stored with tyrosinase in a simple PBS buffer on the glass fiber pads, while others were stored with tyrosinase prepared in PBS containing 20 mg mL^{-1} bovine serum albumin (BSA). In all cases, devices were stored in Petri dishes wrapped with parafilm and covered in aluminum foil. At various time points (1 day, 2 days, 7 days), devices were removed and 20 μL of 10 ppm Ziram was added. The image analysis procedure was followed as described above.

The results showed that the best storage condition was with BSA at −20 °C, where more than 90% of the signal was retained even after a week. This indicates that the enzyme and substrates remain active even after a week under these conditions. Future work will focus on further optimizing the storage conditions to enhance the retention of reagent activity. Additionally, by refining packaging protocols, this system could be developed for point-of-need testing applications,

enabling batch manufacturing, shipping, and refrigeration upon arrival, followed by subsequent use (Fig. 6).

Sensor evaluation through glove extraction

Spike recovery analysis was conducted using glove extraction to demonstrate the sensor's usability for pesticide exposure in real-world testing (Table 1). Two glove types (100% nitrile and cowhide leather) were cut into 10 mm circles using a biopsy punch. Each circle was spiked with three different concentrations and dried at room temperature. The selected concentrations were above the sensor's detection limit but within its linear dynamic range. The dried glove pieces were added to 1 mL of solvent and shaken for 1 minute. After filtration, the samples were analyzed using our fast-flow platform. The spike recovery analysis revealed an extraction efficiency of 82.5% to 87.5% for leather gloves and 68.9% to 71.9% for nitrile gloves. Cotton gloves were also tested with the extraction protocol; however, the method resulted in a loss of structural integrity, making them unsuitable for the study. This extraction efficiency, with a 5% variation across the concentration range, indicates that our sensor has the potential for reliable and precise detection of carbamate pesticide exposure in real-world settings.

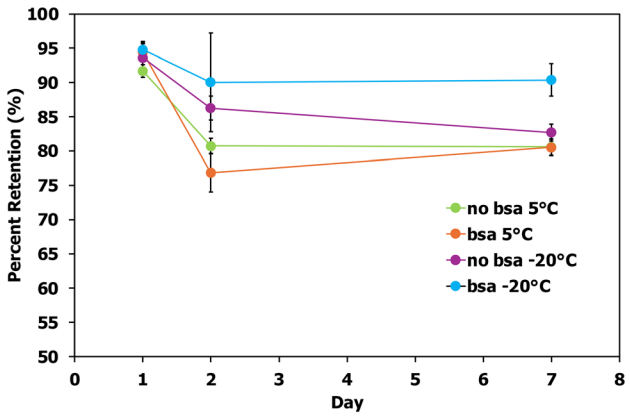

Fig. 6 Stability study of the developed sensor. The day of each test was plotted against the percent retention in signal for each device. All devices were stored in Petri dishes filled with approximately one to two grams of molecular sieves, sealed off with parafilm, and covered in aluminum foil. Devices were tested in a 5 °C fridge and a −20 °C freezer. In each condition, some devices contained tyrosinase in simple PBS buffer on the glass fiber pads, whereas others contained tyrosinase prepared in PBS + 20 mg mL^{-1} bovine serum albumin (BSA).

Table 1 Validation of on-site pesticide detection using glove extraction

Glove type	Spiked (ppm)	Recovered (ppm)	Recovery (%)
Leather	2	1.75 ± 0.39	87.5
	5	4.21 ± 1.00	84.3
	10	8.25 ± 1.86	82.5
Nitrile	2	1.44 ± 0.54	71.9
	5	3.44 ± 0.81	68.9
	10	7.01 ± 0.99	70.1

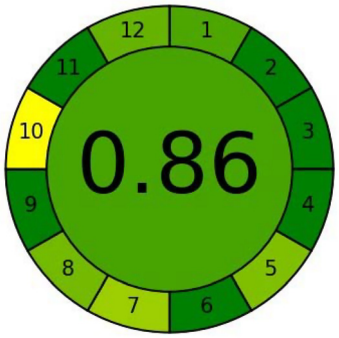

Fig. 7 AGREE criteria report for the developed sensor. An assessment of the greenness of an analytical procedure, in this case, the tyrosinase assay employed on the fast-flow device. 0.86 out of 1 score shows a strong environmentally friendly and safe device for end users to manipulate out in the field. All twelve principles weighted equally.

Sustainability

To evaluate the suitability of our tyrosinase assay for field use, we employed the AGREE (Analytical GREEnness Metric Approach) software, a publicly accessible tool assessing the environmental impact and safety of analytical procedures.[38] The assay achieved a high AGREE score of 0.86 out of 1, indicating a high potential for safe and effective field deployment, even by untrained personnel (Fig. 7). This platform is designed to empower citizens to participate in scientific inquiry while prioritizing public health. By minimizing environmental impact through minimal reagent use, non-toxic chemicals, and incorporating safety features like an enclosed system, and user-friendly interface, we aim to create a reliable and accessible tool. The strong AGREE score reinforces our confidence in the assay's suitability for widespread, responsible use. Further information on the AGREE report is included in the ESI (Fig. S7†).

Conclusion

The capillary-driven microfluidic device developed in this study offers a fast, user-friendly, and cost-effective solution for the on-site detection of dithiocarbamate (DTC) pesticides, addressing the critical need for rapid pesticide monitoring in environmental settings. By integrating hollow channel microfluidics with a paper-based platform, the device significantly reduces the time required to generate a colorimetric signal, enabling near-instantaneous detection of DTCs without the need for complex procedures or specialized equipment. Unlike traditional paper-based platforms, our system transports pesticide samples through hollow capillary channels within seconds without adsorption of pesticides in the microchannels. While much research has focused on acetylcholinesterase inhibition on paper, this study is the first to introduce a tyrosinase inhibition-based assay on a paper platform for pesticide detection. The device demonstrated reliable detection of Ziram, a common DTC pesticide, with a limit of detection

(LoD) of 1.5 ppm. The successful application of the device for Ziram analysis in glove samples, coupled with a spike recovery analysis showing extraction efficiencies ranging from 82.5% to 87.5% for leather gloves and 68.9% to 78.9% for nitrile gloves, highlights its potential for practical, real-world use. Moreover, the device's performance was consistent under various conditions, confirming its stability and reliability for field applications. Future studies will explore the device's stability under ambient conditions, and determine what steps are needed to adapt the device to run sufficiently where refrigeration may not be available. The capillary-driven microfluidic device shows great promise as a low-cost solution for pesticide detection, especially in areas with high pesticide use and limited lab resources. While this study focused on detecting DTCs, the device can be optimized for other analytes and expanded to detect a wider range of pesticides and contaminants. This advancement offers a practical, scalable tool for environmental monitoring and agricultural safety, with future research aimed at improving stability and expanding its capabilities.

Author contributions

CEH and PA contributed to conceptualization, experiments, data curation, formal analysis, methodology, and contributed to writing the original draft as well as reviewing and editing. EB and TA contributed to funding and editing. CSH contributed to the research conceptualization, supervision, funding, and final review and editing.

Data availability

The data that supports the findings of this study are available in the ESI† of this article. The raw data are available on request from the corresponding author.

Conflicts of interest

The authors declare no competing interest.

Acknowledgements

This study was funded through a contract (W911QY2120003) awarded by the US Army DEVCOM Center, and the National Science Foundation (Fellow ID: 2022343709) providing financial support for the research.

References

1 M. Tao, P. R. Adler, A. E. Larsen and S. Suh, *Environ. Res. Lett.*, 2020, **15**, 124049.
2 M. W. Aktar, D. Sengupta and A. Chowdhury, *Inter. Discip. Toxicol.*, 2009, **2**, 1–12.
3 I. Ansari, M. M. El-Kady, C. Arora, M. Sundararajan, D. Maiti and A. Khan, in *Global Climate Change*, 2021, pp. 361–391, DOI: **10.1016/b978-0-12-822928-6.00017-4**.
4 M. Tudi, H. Li, H. Li, L. Wang, J. Lyu, L. Yang, S. Tong, Q. J. Yu, H. D. Ruan, A. Atabila, D. T. Phung, R. Sadler and D. Connell, *Toxics*, 2022, **10**, 335.
5 K. H. Kim, E. Kabir and S. A. Jahan, *Sci. Total Environ.*, 2017, **575**, 525–535.
6 W. Boedeker, M. Watts, P. Clausing and E. Marquez, *BMC Public Health*, 2020, **20**, 1875.
7 B. W. Lee, L. London, J. Paulauskis, J. Myers and D. C. Christiani, *J. Occup. Environ. Med.*, 2003, **45**, 118–122.
8 C. Campanale, M. Triozzi, A. Ragonese, D. Losacco and C. Massarelli, *Toxics*, 2023, **11**, 851.
9 A. K. Malik and W. Faubel, *Pestic. Sci.*, 1999, **55**, 965–970.
10 S. Beshana, A. Hussen, S. Leta and T. Kaneta, *Bull. Environ. Contam. Toxicol.*, 2022, **109**, 344–351.
11 P. Aryal, C. Hefner, B. Martinez and C. S. Henry, *Lab Chip*, 2024, **24**, 1175–1206.
12 P. Murugesan, G. Raj and J. A. Moses, *Rev. Environ. Sci. Bio/Technol.*, 2023, **22**, 625–652.
13 J. S. Van Dyk and B. Pletschke, *Chemosphere*, 2011, **82**, 291–307.
14 B. Rajangam, D. K. Daniel and A. I. Krastanov, *Eng. Life Sci.*, 2018, **18**, 4–19.
15 M. Lafuente, I. Pellejero, A. Clemente, M. A. Urbiztondo, R. Mallada, S. Reinoso, M. P. Pina and L. M. Gandia, *ACS Appl. Mater. Interfaces*, 2020, **12**, 36458–36467.
16 I. Al Yahyai, H. A. J. Al-Lawati and J. Hassanzadeh, *Anal. Methods*, 2021, **13**, 3461–3470.
17 E. C. Reynoso, E. Torres, F. Bettazzi and I. Palchetti, *Biosensors*, 2019, **9**, 20.
18 M. Liu, A. Khan, Z. Wang, Y. Liu, G. Yang, Y. Deng and N. He, *Biosens. Bioelectron.*, 2019, **130**, 174–184.
19 B. Uka, J. Kieninger, G. A. Urban and A. Weltin, *ACS Sens.*, 2021, **6**, 2738–2746.
20 K. H. Wu, W. C. Huang, J. C. Wang and S. H. Wang, *Anal. Methods*, 2024, **16**, 1043–1049.
21 A. M. Bondzic, T. D. Lazarevic-Pasti, A. R. Leskovac, S. Z. Petrovic, M. B. Colovic, T. N. Parac-Vogt and G. V. Janjic, *Eur. J. Pharm. Sci.*, 2020, **151**, 105376.
22 I. Jang, D. B. Carrao, R. F. Menger, A. R. Moraes de Oliveira and C. S. Henry, *ACS Sens.*, 2020, **5**, 2230–2238.
23 C. A. Ramsden and P. A. Riley, *Bioorg. Med. Chem.*, 2014, **22**, 2388–2395.
24 S. Solé, A. Merkoçi and S. Alegret, *Anal. Chem.*, 2003, **33**, 127–143.
25 D. Wang, D. Liu, H. Duan, Y. Xu, Z. Zhou and P. Wang, *J. Agric. Food Chem.*, 2020, **68**, 9252–9259.
26 Y. Guo, X. Zheng, X. Wang, Z. Zhang, S. Qin, X. Wang and X. Jing, *Talanta*, 2023, **260**, 124601.
27 P. Aryal, E. Brack, T. Alexander and C. S. Henry, *Anal. Chem.*, 2023, 5820–5827.
28 P. Aryal, A. W. Indrianingsih and C. S. Henry, *Green Anal. Chem.*, 2024, **8**, 100091.
29 C. Prakobdi, T. A. Baldo, P. Aryal, J. Link, P. Saetear and C. S. Henry, *Anal. Methods*, 2024, **16**, 2489–2495.

30 P. Aryal, J. Boes, E. Brack, T. Alexander and C. S. Henry, *ACS Sens.*, 2024, **9**, 5479–5488.
31 M. T. Alam, V. Olin-Sandoval, A. Stincone, M. A. Keller, A. Zelezniak, B. F. Luisi and M. Ralser, *Nat. Commun.*, 2017, **8**, 16018.
32 D. J. Anderson, *Clin. Chem.*, 1989, **35**, 2152–2153.
33 A. Craig, *Br. J. Cancer*, 1977, **36**, 432.
34 M. Pabbi, A. Kaur, S. K. Mittal and R. Jindal, *Sens. Actuators, B*, 2018, **258**, 215–227.
35 F. Arduini, F. Ricci, I. Bourais, A. Amine, D. Moscone and G. Palleschi, *Anal. Lett.*, 2005, **38**, 1703–1719.
36 S. H. Lee, I. H. Bae, E. S. Lee, H. J. Kim, J. Lee and C. S. Lee, *Int. J. Mol. Sci.*, 2020, **21**, 1736.
37 Y. T. Yu, L. Zhong, Q. He, F. Chen, H. Wu, Y.-P. Chen, P. P. Piccaluga and S. Xie, *BIO Web Conf.*, 2024, **111**, 03018.
38 F. Pena-Pereira, W. Wojnowski and M. Tobiszewski, *Anal. Chem.*, 2020, **92**, 10076–10082.